ANISOTROPIC MESH ADAPTATION FOR FINITE VOLUME AND FINITE ELEMENT METHODS ON TRIANGULAR MESHES

Vít Dolejší
Departement of Numerical Mathematics,
Faculty of Mathematics and Physics,
Charles University,
Malostranské nám. 25,
118 00 Prague - Czech Republic

Abstract

The present paper deals with an anisotropic mesh adaptation (AMA) of triangulation which can be employed for the numerical solution various problems of physics. AMA tries to construct an optimal triangulation of the domain of computation in the sense that an "error" of the solution of the problem considered is uniformly distributed over the whole triangulation. First, we describe the main idea of AMA. We define an optimal triangle and an optimal triangulation. Then we describe the process of optimization of the triangulation and the complete multilevel computational process. We apply AMA to a problem of CFD, namely to inviscid compressible flow. The computational results for a channel flow are presented.

Key words: Mesh adaptation – Riemann metric – unstructured mesh – compressible flows

1 Introduction

The *finite volume* and/or *finite element methods* are very often employed for solving various problems of physics (for example fluid mechanics, elasticity, heat conduction, etc.). Here, the computational domain is divided into a finite number of triangles and the system of partial differential equations describing the problem is discretized. To obtain an accurate numerical solution, a fine triangulation has, to be used. On the other hand, a very fine triangulation gives a large number of elements and the computation requires a lot of memory and CPU time. This was the reason why adaptative methods were developed. We seek the subdomains where the numerical solution is inaccurate and we refine the triangulation there. A standard technique is the *red–green refinement*: we define an indicator and triangles with values of the indicator greater than a tolerance prescribed are refined. The red–green strategy gives good results but the number of elements after n refinements (n equals, for example, 3, 4 or 5) is very large. Another possibility is to use *the anisotropic mesh adaptation* (AMA) where we can obtain the same quality of solution, using a less number of elements. AMA can not only refine the triangulation but also removes some triangles and moves the nodes of mesh. So we can obtain a triangulation with a not too large number of elements on which a sufficiently accurate solution can be computed.

AMA tries to construct an optimal mesh in the sense that an "error" of the solution of the problem considered is uniformly distributed over the whole triangulation. In distinction to the red–green refinement technique, AMA allows for the refinement of triangles in a special direction. E.g., it is possible to align the refinement along a discontinuity. This requires to have some error indicator which detects not only the value of error but also the changes of error with respect to the direction. Such an indicator can be represented by a set of 2×2 symmetric and positive definite matrices M_i which also represent the Riemann metric in the domain Ω of computation.

The main idea of AMA is given in Section 2. In Section 3 we define *the optimal triangle corresponding to a matrix*, in Section 4 we define *the optimal triangulation*. The construction of the optimal triangulation is described in Section 5. In Section 6 we describe the generation of matrices M and in Section 7 we describe the multilevel computation using AMA. The last section presents some numerical results for CFD problems.

2 Interpolation error

Here we describe the main idea of AMA. Let u be an analytical solution of a considered problem and u_h be its piecewise linear approximation. Our aim is to construct a triangulation $\mathcal{T}$ of a computational domain Ω so that the *interpolation error* (see [4]) $e_I(x,y) \equiv |u(x,y) - u_h(x,y)|,\ (x,y) \in \Omega$ is for each $(x,y) \in \Omega$ smaller than given tolerance and on the other hand the number of elements of triangulation is not high.

Let $u \in C^2(\Omega)$. Then, using the Taylor series expansion at $(x_0,y_0) \in \Omega$, we have

$$\begin{aligned} u(x,y) &= u(x_0,y_0) + \frac{\partial u(x_0,y_0)}{\partial x}(x-x_0) + \frac{\partial u(x_0,y_0)}{\partial y}(y-y_0) + \qquad (1)\\ &+ \frac{1}{2}\left[\frac{\partial^2 u(x_0,y_0)}{\partial x^2}(x-x_0)^2 + 2\frac{\partial^2 u(x_0,y_0)}{\partial x \partial y}(x-x_0)(y-y_0) + \frac{\partial^2 u(x_0,y_0)}{\partial y^2}(y-y_0)^2\right] + \\ &+ o(|x-x_0, y-y_0|^2) \quad (x,y) \in \Omega. \end{aligned}$$

Now we define the linear approximation of u in some neighbourhood $\mathcal{U}((x_0,y_0)) \subset \Omega$ of (x_0,y_0) by

$$\begin{aligned} u_h|_{\mathcal{U}((x_0,y_0))}(x,y) &:= u(x_0,y_0) + \frac{\partial u(x_0,y_0)}{\partial x}(x-x_0) + \frac{\partial u(x_0,y_0)}{\partial y}(y-y_0), \qquad (2)\\ & \qquad (x,y) \in \mathcal{U}((x_0,y_0)). \end{aligned}$$

Then for the interpolation error in $\mathcal{U}((x_0,y_0))$ we obtain by (we omit the terms of order $o(|x-x_0,y-y_0|^2)$)

$$\begin{aligned} e_{\mathrm{I}}\ |_{\mathcal{U}((x_0,y_0))}(x,y) &:= \left|u(x,y) - u_h|_{\mathcal{U}((x_0,y_0))}(x,y)\right| \approx \qquad (3)\\ &\approx \frac{1}{2}\left|\frac{\partial^2 u(x_0,y_0)}{\partial x^2}(x-x_0)^2 + 2\frac{\partial^2 u(x_0,y_0)}{\partial x \partial y}(x-x_0)(y-y_0) + \frac{\partial^2 u(x_0,y_0)}{\partial y^2}(y-y_0)^2\right|, \end{aligned}$$

which is valid for $(x,y) \in \mathcal{U}((x_0,y_0))$. If $\omega > 0$ is a given tolerance, we require that $e_I(x,y) \leq \omega$. This and (3) give

$$\left|\frac{\partial^2 u(x_0,y_0)}{\partial x^2}(x-x_0)^2 + 2\frac{\partial^2 u(x_0,y_0)}{\partial x \partial y}(x-x_0)(y-y_0) + \frac{\partial^2 u(x_0,y_0)}{\partial y^2}(y-y_0)^2\right| \leq 2\omega, \qquad (4)$$

which can be rewritten as

$$\begin{pmatrix} x-x_0, & y-y_0 \end{pmatrix} \cdot \left.\begin{pmatrix} \frac{\partial^2 u}{\partial x^2} & \frac{\partial^2 u}{\partial x \partial y} \\ \frac{\partial^2 u}{\partial x \partial y} & \frac{\partial^2 u}{\partial y^2} \end{pmatrix}\right|_{(x_0,y_0)} \begin{pmatrix} x-x_0 \\ y-y_0 \end{pmatrix} \leq 2\omega \qquad (5)$$

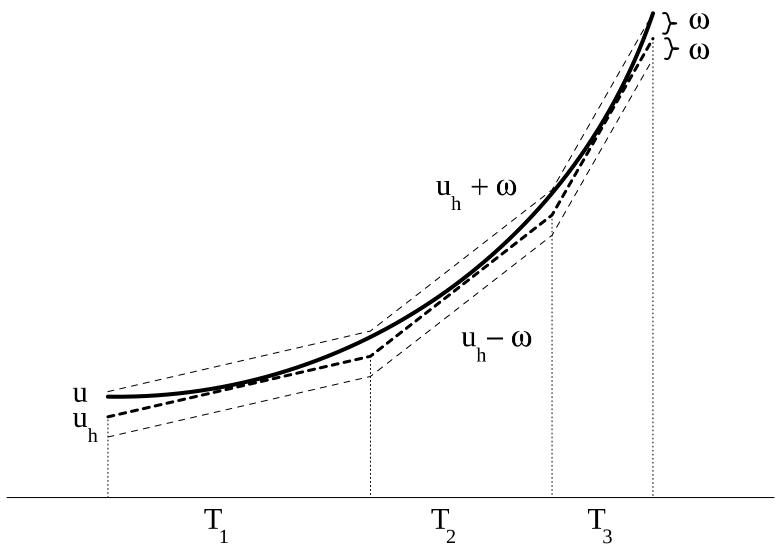

Figure 1: "Triangulation" for 1–D case satisfying the condition (6)."Elements" T_1, T_2, T_3, exact solution u (solid line), approximate solution u_h (dashed line).

provided that the Hessian matrix from (5) is positive definite. Under this assumption the points (x, y) satisfying the relation (5) form an ellipse $\epsilon(\omega) \subset I\!R^2$. From this it follows that the interpolation error $e_I(x, y)$ is less or equal to ω for all $(x, y) \in \epsilon(\omega)$. Furthermore, if T is such a triangle that $T \subset \epsilon(\omega)$, then $e_I(x, y) \leq \omega$ for all $(x, y) \in T$. To have a good triangulation (i.e. with the number of triangles not too high) we chose such triangle which is a subset of $\epsilon(\omega)$ and has the maximal possible area. If the triangulation is formed by the triangles with the above properties (for each triangle we have another matrix) then the required condition will be satisfied:

$$e_{\rm I}(x, y) = |u(x, y) - u_h(x, y)| \leq \omega \quad \forall (x, y) \in \Omega. \tag{6}$$

Here u_h arises as composition of functions of type (2). The above consideration are illustrated in Fig. 1 for 1–D case. The interpolation error can be locally represented by a matrix from (5) which defines the Riemann metric.

There are some problems in the previous consideration. First, the function u is not generally smooth ($u \notin C^2(\Omega)$). Further, the matrix from (5) is not positive definite in general. Finally, if the analytical solution is (locally) linear, then the interpolation error given by (3) vanishes and the ellipse $\epsilon(\omega)$ does not exist. In the following sections we describe an iterative process for a construction of a triangulation where we must avoid the problems mentioned above.

3 Optimal triangle

We will define an optimal triangle corresponding to the matrix M representing the Riemann metric which we have mentioned in the previous section. Here we do not specify the matrix from (5) (for the definition of M see Section 6). Let M be a symmetric and positive definite 2×2 matrix

$$M = \begin{pmatrix} a & b \\ b & c \end{pmatrix}, \qquad ac - b^2 > 0, \tag{7}$$

and let $\boldsymbol{v} = (v_1, v_2)$ be a vector in $I\!R^2$. We define *the norm* of the vector $\boldsymbol{v}$ *corresponding* to the matrix M as

$$\|\boldsymbol{v}\|_M \equiv \left(\boldsymbol{v} M \boldsymbol{v}^T\right)^{\frac{1}{2}} = \left[\begin{pmatrix} v_1 & v_2 \end{pmatrix}\begin{pmatrix} a & b \\ b & c \end{pmatrix}\begin{pmatrix} v_1 \\ v_2 \end{pmatrix}\right]^{\frac{1}{2}} = \left(a v_1^2 + 2 b v_1 v_2 + c v_2^2\right)^{\frac{1}{2}}. \qquad (8)$$

If $M = I$ (=identical matrix) then $\|\boldsymbol{v}\|_M = |\boldsymbol{v}|$, where $|\boldsymbol{v}| = (v_1^2 + v_2^2)^{1/2}$. The matrix M can be interpreted as *an error matrix* and the norm $\|\boldsymbol{v}\|_M$ as an error of solution over the edge $\boldsymbol{v}$ (see [1], [9]).

We decompose M in the following way:

$$M \equiv \begin{pmatrix} a & b \\ b & c \end{pmatrix} = R^T \Lambda R = \begin{pmatrix} \cos\theta & \sin\theta \\ -\sin\theta & \cos\theta \end{pmatrix}\begin{pmatrix} \lambda_1 & 0 \\ 0 & \lambda_2 \end{pmatrix}\begin{pmatrix} \cos\theta & -\sin\theta \\ \sin\theta & \cos\theta \end{pmatrix}, \qquad (9)$$

where λ_1, λ_2 are the eigenvalues of M and $\theta \in [0, 2\pi)$.

Let Oxy be a Cartesian coordinate system. By ϵ_M we denote an ellipse with the axes lengths $r_1 = 1/\sqrt{\lambda_1}, r_2 = 1/\sqrt{\lambda_2}$. The angle between the axis x and the major axis of ϵ_M is θ. (See Fig. 2 .) If P_0 is the center of ϵ_M, then it is easy to see that for any point P lying on the boundary of ϵ_M the norm of the vector $P_0P = (P - P_0)$ corresponding to M is constant and $\|P_0P\|_M = 1$. In comparison to Section 2 we can consider $\|P_0P\|_M$ as the interpolation error in P (P_0 corresponds to (x_0, y_0)). Then ϵ_M consists of points with the same interpolation error.

We define *the optimal triangle* T_M *corresponding to* M such that $T_M \subset \epsilon_M$ and $|T_M| \geq |T|$ for any triangle $T \subset \epsilon_M$. (Here $|T|$ means the area of the triangle T). If $M = I$ (= unit matrix) then ϵ_M is an unit circle and T_M is an equilateral triangle with the lengths of edges equal to $\sqrt{3}$.

Now we express analytically the coordinates of the optimal triangle T_M. Let us define a new Cartesian coordinate system $\tilde{O}\tilde{x}\tilde{y}$ with the center at the center of ϵ_M and with the axes parallel with the axes of the ellipse (Fig. 3).

The problem of finding a triangle contained in ϵ_M with the maximal area has 4 solutions. These four triangles have the following vertices:

$$\tilde{V}_1^{(1)} = \left[\frac{1}{\sqrt{\lambda_1}}, 0\right], \quad \tilde{V}_2^{(1)} = \left[-\frac{1}{2}\frac{1}{\sqrt{\lambda_1}}, \frac{\sqrt{3}}{2}\frac{1}{\sqrt{\lambda_2}}\right], \quad \tilde{V}_3^{(1)} = \left[-\frac{1}{2}\frac{1}{\sqrt{\lambda_1}}, -\frac{\sqrt{3}}{2}\frac{1}{\sqrt{\lambda_2}}\right], \qquad (10)$$

$$\tilde{V}_1^{(2)} = \left[-\frac{1}{\sqrt{\lambda_1}}, 0\right], \quad \tilde{V}_2^{(2)} = \left[\frac{1}{2}\frac{1}{\sqrt{\lambda_1}}, -\frac{\sqrt{3}}{2}\frac{1}{\sqrt{\lambda_2}}\right], \quad \tilde{V}_3^{(2)} = \left[\frac{1}{2}\frac{1}{\sqrt{\lambda_1}}, \frac{\sqrt{3}}{2}\frac{1}{\sqrt{\lambda_2}}\right], \qquad (11)$$

$$\tilde{V}_1^{(3)} = \left[\frac{1}{\sqrt{\lambda_2}}, 0\right], \quad \tilde{V}_2^{(3)} = \left[-\frac{1}{2}\frac{1}{\sqrt{\lambda_2}}, \frac{\sqrt{3}}{2}\frac{1}{\sqrt{\lambda_1}}\right], \quad \tilde{V}_3^{(3)} = \left[-\frac{1}{2}\frac{1}{\sqrt{\lambda_2}}, -\frac{\sqrt{3}}{2}\frac{1}{\sqrt{\lambda_1}}\right], \qquad (12)$$

$$\tilde{V}_1^{(4)} = \left[-\frac{1}{\sqrt{\lambda_2}}, 0\right], \quad \tilde{V}_2^{(4)} = \left[\frac{1}{2}\frac{1}{\sqrt{\lambda_2}}, -\frac{\sqrt{3}}{2}\frac{1}{\sqrt{\lambda_1}}\right], \quad \tilde{V}_3^{(4)} = \left[\frac{1}{2}\frac{1}{\sqrt{\lambda_2}}, \frac{\sqrt{3}}{2}\frac{1}{\sqrt{\lambda_1}}\right]. \qquad (13)$$

Then the area of all these triangles $\tilde{V}_1^{(l)}\tilde{V}_2^{(l)}\tilde{V}_3^{(l)}$, $l = 1, \ldots, 4$ is equal to

$$|T_M| = \frac{3\sqrt{3}}{4}\frac{1}{\sqrt{\lambda_1\lambda_2}}. \qquad (14)$$

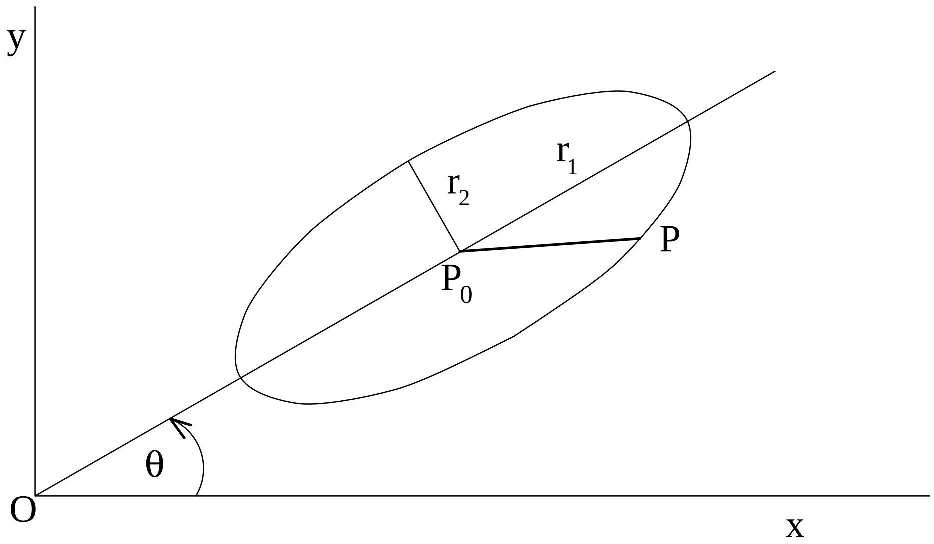

Figure 2: An ellipse ϵ_M corresponding to M with semiaxes length r_1, r_2, P_0 center of ϵ_M, P any point of ϵ_M.

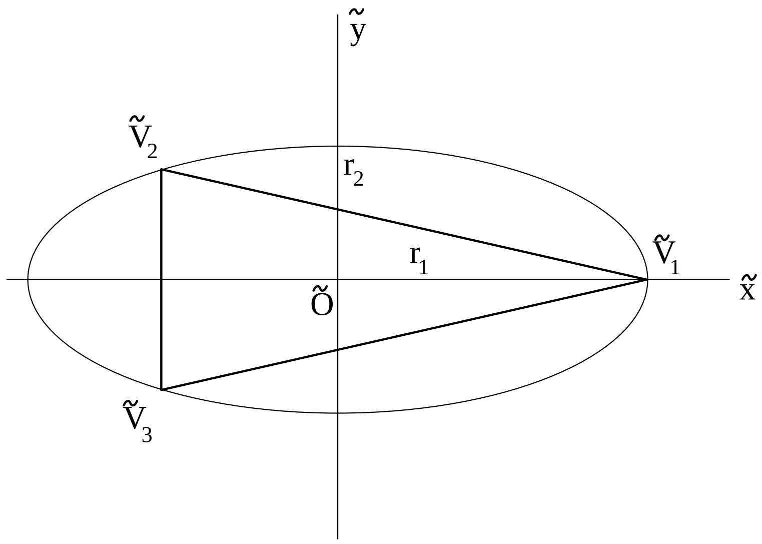

Figure 3: An ellipse ϵ_M corresponding to M in the new Cartesian system and the optimal triangle $T_M = \tilde{V}_1\tilde{V}_2\tilde{V}_3$.

Fig. 3 shows the optimal triangle $\tilde{V}_1^{(1)}\tilde{V}_2^{(1)}\tilde{V}_3^{(1)}$. The lengths of edges in the direction $\tilde{y}$ are smaller than the lengths of edges in the direction $\tilde{x}$.

Now we can go back to the original coordinate system by the transformation

$$V = R\tilde{V} + d, \tag{15}$$

where V is a point in the system Oxy, $\tilde{V}$ is a point in the system $\tilde{O}\tilde{x}\tilde{y}$, R is the matrix of the rotation from (9) and $d = (d_1, d_2)$ is the position of the center of ϵ_M in the coordinate system $\tilde{O}\tilde{x}\tilde{y}$. Applying (15) to the points $\tilde{V}_1, \tilde{V}_2, \tilde{V}_3$ (here we use the transformation only for the first triangle given by (10) and we omit the superscript $^{(1)}$) we obtain the points V_1, V_2, V_3 which are the vertices of the optimal triangle T_M in the original system:

$$\begin{aligned}
V_1 &= \left[\frac{\cos\theta}{\sqrt{\lambda_1}}, \frac{\sin\theta}{\sqrt{\lambda_2}}\right] + [d_1, d_2] \\
V_2 &= \left[-\frac{\sqrt{3}}{2}\frac{\sqrt{\lambda_2}\cos\theta + \sqrt{\lambda_1}\sin\theta}{\sqrt{\lambda_1\lambda_2}}, \frac{\sqrt{3}}{2}\frac{\sqrt{\lambda_1}\cos\theta - \sqrt{\lambda_2}\sin\theta}{\sqrt{\lambda_1\lambda_2}}\right] + [d_1, d_2], \\
V_3 &= \left[-\frac{\sqrt{3}}{2}\frac{-\sqrt{\lambda_2}\cos\theta + \sqrt{\lambda_1}\sin\theta}{\sqrt{\lambda_1\lambda_2}}, \frac{\sqrt{3}}{2}\frac{\sqrt{\lambda_1}\cos\theta + \sqrt{\lambda_2}\sin\theta}{\sqrt{\lambda_1\lambda_2}}\right] + [d_1, d_2].
\end{aligned}$$

Now we compute the norms corresponding to M of the sides of T_M. We put $\boldsymbol{v}_1 = V_1 - V_2,\ \boldsymbol{v}_2 = V_2 - V_3,\ \boldsymbol{v}_3 = V_3 - V_1$. After some elementary but long calculation we find that

$$\|\boldsymbol{v}_i\|_M = \left(\boldsymbol{v}_i M \boldsymbol{v}_i^T\right)^{\frac{1}{2}} = \sqrt{3}, \qquad i = 1, 2, 3, \tag{16}$$

i.e. the norms of all sides of the optimal triangle T_M are constant and equal to $\sqrt{3}$. The relation (16) is valid also for triangles which we obtain applying (15) to (11), (12) and (13). This is a very interesting and important property in the context of AMA. In the following we will not consider an optimal triangle as a triangle which is subset of ϵ_M and has the maximal possible area but as a triangle with property (16).

4 Optimal mesh

Here we define an optimal triangulation not as a set of optimal triangles but we use the property (16). This approach is more suitable for a numerical realization.

Let $\mathcal{T}$ be a triangulation of the computational domain Ω. Let M_i be a symmetric positive definite 2×2 matrix defined for each node P_i, $i \in I(=$ an index set$)$, of the triangulation $\mathcal{T}$. Then for each edge of the triangulation S_j, $j \in J(=$ an index set$)$, we put $\bar{M}_j := \frac{1}{2}(M_{j_1} + M_{j_2})$ where P_{j_1}, P_{j_2} are the initial and final points forming S_j, and M_{j_1}, M_{j_2} are the corresponding matrices. Now, we say that the mesh $\mathcal{T}$ is *optimal*, if the norm of S_j corresponding to $\bar{M}_j$ is equal to $\sqrt{3}$ for all $j \in J$, i.e.

$$\|S_j\|_{\bar{M}_j} = \sqrt{3} \qquad \forall j \in J. \tag{17}$$

It means that the error (considered as $\|\cdot\|_M$) for each edge of $\mathcal{T}$ is the same, i.e., it is uniformly distributed over the triangulation.

Let $M_i = \bar{c}I$, $i \in I$, where $\bar{c}$ is some constant. Then the optimal mesh is uniform, i.e., not only the norms of all edges of all triangles are the same but also their lengths (in the

Euclidean metric) are the same (because $\|\boldsymbol{v}\|_{M_i} = \sqrt{c}|\boldsymbol{v}|,\ i \in I$) which implies that the inner angles of all triangles are equal to $\pi/3$. It is easy to see that the optimal mesh exists only for special types of domains Ω, for example if Ω is an equilateral triangle. On the other hand, if $\Omega = [0,1] \times [0,1]$ the optimal triangulation does not exist because the angle of triangles at the corners of the domain cannot be equal to $\pi/3$. We will try to construct the mesh which will be close to the optimal one.

We define *the quality parameter of a triangle* $T_n \in \mathcal{T}$ by

$$q_{T_n} = \sum_{l=1}^{3} \left(\|\boldsymbol{v}_{nl}\|_{\bar{M}_{nl}} - \sqrt{3} \right)^2, \tag{18}$$

where $\|\boldsymbol{v}_{nl}\|_{\bar{M}_{nl}},\ l = 1,2,3$, are the norms of the sides of the triangle T_n. We define *the quality parameter* $Q_{\mathcal{T}}$ of the mesh $\mathcal{T}$ by

$$Q_{\mathcal{T}} = \frac{1}{nelem} \sum_{T_n \in \mathcal{T}} q_{T_n}, \tag{19}$$

where q_{T_n} is the quality parameter of triangle T_n and $nelem$ is a number of triangles in $\mathcal{T}$. It is clear that $Q_{\mathcal{T}} \geq 0$ always and if the mesh $\mathcal{T}$ is optimal then $Q_{\mathcal{T}} = 0$. $Q_{\mathcal{T}}$ is a measure how close the triangulation $\mathcal{T}$ is to the optimal one. We will construct a mesh for which the quality parameter $Q_{\mathcal{T}}$ is minimal.

5 Optimization of the mesh

In this section we describe a procedure for the construction of a mesh which will be an approximation of the optimal one (because the optimal triangulation does not exist in general). We start from some initial triangulation $\mathcal{T}_{\text{init}}$ whose quality we want to improve.

Let us suppose that we have a triangulation $\mathcal{T}_{\text{int}}$ with matrices $M_i,\ i \in I$ (M_i symmetric and positive definite). We want to find a new triangulation $\mathcal{T}_{\text{new}}$ such that $Q_{\mathcal{T}_{\text{new}}}$ is minimal. To obtain $\mathcal{T}_{\text{new}}$, an iterative process is used. Each iteration consists of a certain number of the following local operations:

- adding a node at the center of an edge,
- removing an edge,
- swapping the diagonal of the quadrilateral formed by any pair of adjacent elements,
- moving a node.

Now we describe more precisely these local operations.

5.1 Adding a node

If the norm of some edge of a triangle is greater than a prescribed constant $L_{\max}$ we put a new node at the center of this edge (Fig. 4). Here the norm of the edge AC is greater than $L_{\max}$ and, therefore, the node E is inserted at the center of AC.

We use $L_{\max} = \sqrt{16/3}$. If $\|\boldsymbol{v}\|_M > L_{\max}$ for some $\boldsymbol{v}$ then we have $\left| \|\boldsymbol{v}\|_M - \sqrt{3} \right| > \left| \|\boldsymbol{v}\|_M/2 - \sqrt{3} \right|$, which means that after adding a node, two edges with the norms $\|\boldsymbol{v}\|_M/2$

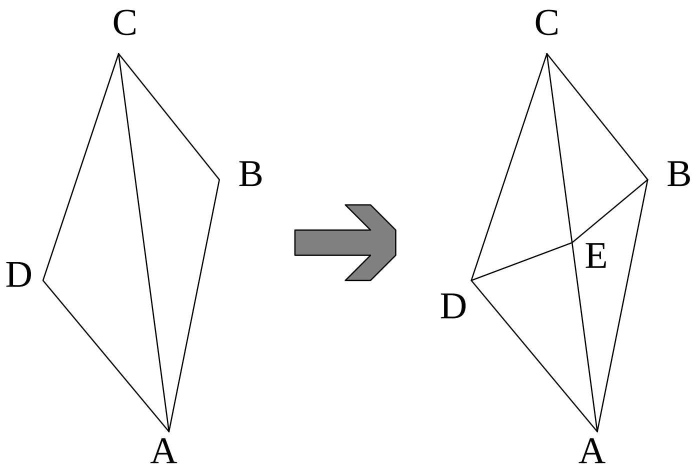

Figure 4: Adding a node E at the center of AC.

arise and the difference $\|\boldsymbol{v}\|_M/2$ and $\sqrt{3}$ is smaller than the difference of $\|\boldsymbol{v}\|_M$ and $\sqrt{3}$. The changes in the numbers of nodes, elements, and edges are given in the following table.

type of divided edge	nodes	elements	edges
boundary	+1	+1	+2
non–boundary	+1	+2	+3

We must define the matrix M for the new node. If we insert E on the edge AC we put $M_E = \frac{1}{2}(M_A + M_C)$. We denote by $\mathcal{A}$ one application of the adding of nodes at the centers of all edges with the norms greater than $L_{\max}$ to a given triangulation (i.e., each edge can be divided during $\mathcal{A}$ only once).

5.2 Removing an edge

If the norm of some edge of a triangle is smaller than a prescribed constant $L_{\min}$ we remove this edge (Fig. 5). Here the norm of the edge AB is smaller than $L_{\min}$ and, therefore, this edge is removed, i.e., the nodes A, B pass into a new node E. The position of the new point E depends on the position of A and B. If A and B are not on the boundary of Ω we can place E at the center of AB. But if A is a boundary node and B is a non–boundary node we must put $E = A$ so that the boundary would not change. Similarly, if A is a non–boundary node and B is a boundary node we put $E = B$.

We use $L_{\min} = \sqrt{4/3}$, which follows from a similar consideration as in Section 5.1 and is based heuristically on the implication $\left|\|\boldsymbol{v}\|_M - \sqrt{3}\right| > \left|2\|\boldsymbol{v}\|_M - \sqrt{3}\right| \Rightarrow \|\boldsymbol{v}\|_M < \sqrt{4/3}$. The changes in the numbers of nodes, elements, and edges are given in the following table.

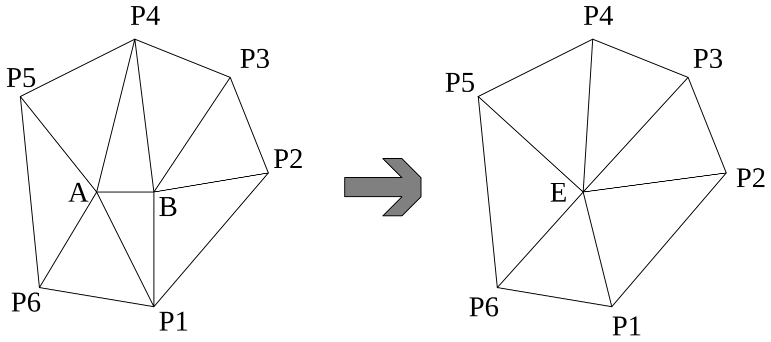

Figure 5: Removing the edge AB and the rise a node E.

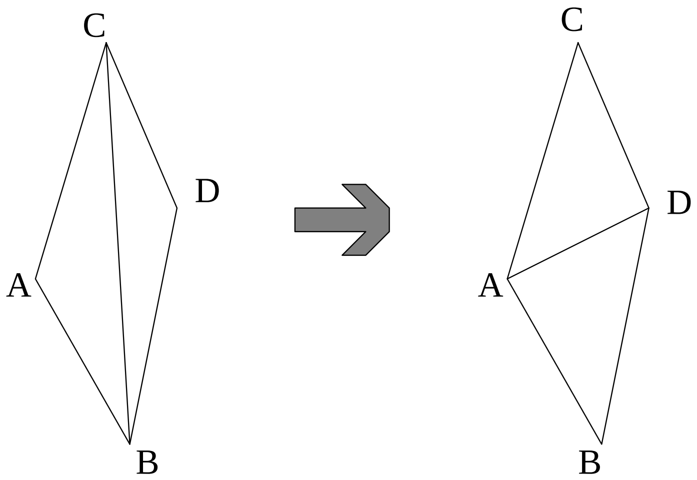

Figure 6: Swapping the diagonal of the quadrilateral formed by pair of adjacent triangles.

type of divided edge	nodes	elements	edges
boundary	-1	-1	-2
non–boundary	-1	-2	-3

We must define the matrix M for the new node. If we put E at the center of the edge AB then we set $M_E = (M_A + M_B)/2$. If we put $E = A$ (or B) we set $M_E = M_A$ (or $M_E = M_B$). We denote by $\mathcal{R}$ one application of the removing of all edges with norms smaller than $L_{\min}$ to a given triangulation.

5.3 Swapping the diagonal

Let ABC and BDC be two adjacent triangles with the common edge BC. Then we can replace the diagonal BC of the quadrilateral $ABCD$ by the diagonal AD and we obtain the triangles ABD and ADC (Fig. 6).

The swapping is performed only if the parameter quality $Q_{\mathcal{T}}$ decreases, i.e., $q_{ABD}+q_{ADC} < q_{ABC} + q_{BDC}$ (for the definition of q, see (18)). The numbers of nodes, elements, and edges

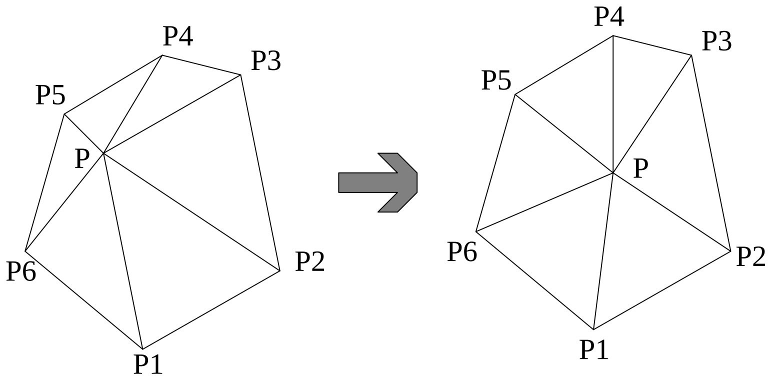

Figure 7: Moving the node P to the new position.

remain the same. We denote by $\mathcal{S}$ the loop over elements consisting of the successive swapping of diagonals as long as $Q_{\mathcal{T}}$ decreases. (The positions of all nodes are fixed.)

5.4 Moving a node

The moving of nodes is not a discrete operation. This operation helps us to "smooth" the triangulation. Let P be a node of the triangulation $\mathcal{T}$. Let $P_1, P_2, \ldots, P_m$ be such nodes that PP_iP_{i+1}, $i = 1, \ldots, m$, $(P_{m+1} \equiv P_1)$ are the triangles from $\mathcal{T}$ (m is the number of these triangles, see Fig. 7). Now the nodes $P_1, P_2, \ldots, P_m$ are fixed and we move the node P. Let P_i^*, $i = 1, \ldots, m$, be such a point that the quality parameter q_{T^i} of the triangle $T^i = P_i^* P_i P_{i+1}$ is minimal for the given position of P_i, P_{i+1} and the given orientation of PP_iP_{i+1}. By the orientation of the triangle ABC we understand the sign of the determinant

$$\begin{pmatrix} x_A & y_A & 1 \\ x_B & y_B & 1 \\ x_C & y_C & 1 \end{pmatrix}, \tag{20}$$

where $[x_A, y_A], [x_B, y_B]$, and $[x_C, y_C]$ are the coordinates of A, B, and C. Using approach given in [2], we have

$$P_i^* = \frac{\begin{pmatrix} d-b & -c \\ a & d+b \end{pmatrix} \cdot (P_{i+1} - P_i)^T}{2d}, \tag{21}$$

where $d = \left((ac - b^2)/3\right)^{1/2}$, and a, b, and c are the elements of the matrix M given by (7). Then we put

$$P^* = \frac{1}{m} \sum_{i=1}^{m} P_i^*. \tag{22}$$

Let $P'(s)$ be a point such that $P'(s) = P + s(P^* - P)$, $s \in [0,1]$. If we move P into $P'(s)$, we obtain a triangulation $\mathcal{T}(s)$ with the quality parameter $Q_{\mathcal{T}}(s)$. We find $s^* \in [0,1]$ such that $Q_{\mathcal{T}}(s^*) \leq Q_{\mathcal{T}}(s)$ for all $s \in [0,1]$ and the new position of P is $P := P'(s^*)$.

The numbers of nodes, elements, and edges remain the same. We denote by $\mathcal{M}$ the application of moving of all nodes in such a way that the quality parameter $Q_{\mathcal{T}}$ is minimal for the given configuration (i.e., during the moving, any swapping, inserting, and removing is not performed).

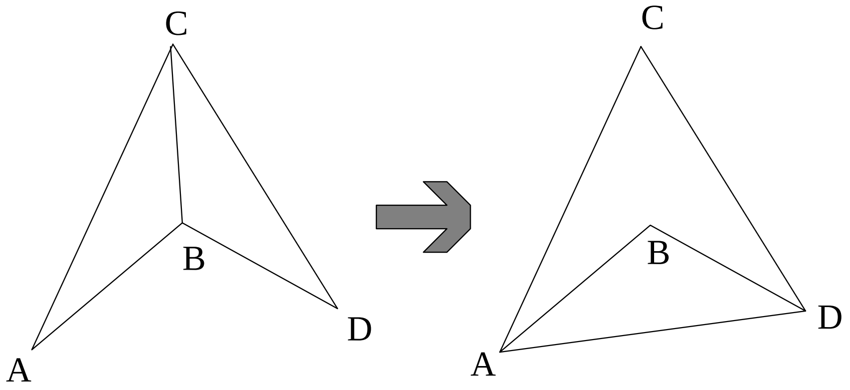

Figure 8: Prohibited case for swapping.

5.5 Boundary nodes

We have to take into account the boundary of the physical domain Ω when adding a node, removing an edge, and moving a node. We have to obey some rules. After each local operation, the boundary of $\mathcal{T}$ must be a polygonal approximation of $\partial\Omega$. We have the list of points lying on $\partial\Omega$ for each problem and we select suitable nodes from this list.

5.6 Minimal angle condition

Many theorems concerning FVM and FEM require that the condition, that there exists a positive constant β such that the magnitude of all angles of all triangles is greater than β, be fulfilled. This condition is equivalent (see [3]) to the existence of $c_1 > 0$ such that

$$h_l^2 \le c_1 |T|, \quad l = 1,2,3, \quad T \in \mathcal{T}, \tag{23}$$

where $h_l,\ l = 1,2,3$, are the lengths of edges of T. This condition should be satisfied also for the triangulation generated by AMA. Therefore, each of the local operations is performed if for a given $\gamma > 0$, the condition

$$\frac{\det \begin{pmatrix} x_A & y_A & 1 \\ x_B & y_B & 1 \\ x_C & y_C & 1 \end{pmatrix}}{|V_A - V_B|^2 + |V_B - V_C|^2 + |V_C - V_A|^2} \ge \gamma \tag{24}$$

is satisfied for each triangle which arises after a local operation. Here, $V_A = (x_A, y_A), V_B = (x_B, y_B)$, and $V_C = (x_C, y_C)$ are the vertices of a triangle from $\mathcal{T}$. The magnitude of the determinant in numerator is the double area of the triangle $V_A V_B V_C$. This condition also verifies whether the orientation of nodes in a triangle is preserved (for the definition of orientation see the text before (20)). This can appear in the swapping where we must avoid the case described in Fig. 8. The swapping is prohibited in Fig. 8 in virtue of (24) because the determinant of the triangle ABD is negative in this case. In our code we put $\gamma = 0.12$.

5.7 Iterative process

We have tried to find the optimal strategy by the combination of the above operations $\mathcal{A}, \mathcal{R}, \mathcal{S}$, and $\mathcal{M}$. Based on numerical experiments, one of the best strategies seems to be the process represented by the formula

$$\mathcal{S} + m \times [\mathcal{M} + \mathcal{S} + \mathcal{R} + \mathcal{M} + \mathcal{A} + \mathcal{M} + \mathcal{S}] + \mathcal{M} \tag{25}$$

(the sequence of operations goes from the left to the right), where m is an integer denoting the number of repetitions of the sequence of operations in the square brackets and its value is chosen in such a way that the sequence in the square bracket is applied until all local operations are performed, i.e., in the last sequence of operations, in the square brackets no edge has been removed, no node has been inserted, and no diagonal has been swapped. We prescribe also a constant $m_{\max}$ and the iterative process is finished if $m \geq m_{\max}$. Our experience gives m equal approximately to 10.

6 Generation of the matrix M

The previous section describes the construction of a triangulation $\mathcal{T}_{\text{new}}$ if we know $\mathcal{T}_{\text{old}}$ and the matrices M_i (symmetric and positive definite) are given for each node of $\mathcal{T}_{\text{old}}$. Now we define how to obtain the matrices M_i. We have defined the interpolation error in Section 2 which can be represented by a Hessian matrix. This matrix is used for the generation of M_i, but we must avoid the problems mentioned in Section 2 (see also [1]).

Let $\boldsymbol{H}_i,\ i \in I$, be a Hessian of some physical quantity η which is characteristic for the problem of consideration (for example, in CFD we put $\eta := \rho$, where ρ is a density of flow). We decompose $\boldsymbol{H}_i$ in the following way:

$$\boldsymbol{H}_i = \left(\begin{array}{cc} \frac{\partial^2 \eta}{\partial x^2} & \frac{\partial^2 \eta}{\partial x \partial y} \\ \frac{\partial^2 \eta}{\partial x \partial y} & \frac{\partial^2 \eta}{\partial y^2} \end{array} \right) \Bigg|_{P_i} = R_i \left(\begin{array}{cc} \Lambda_{i1} & 0 \\ 0 & \Lambda_{i2} \end{array} \right) R_i^{-1} \quad i \in I. \tag{26}$$

(For the computation of the second order derivatives see Section 6.1). The matrices $\boldsymbol{H}_i$ are not suitable as the Riemann metric, because they are not positive definite. Therefore, we put

$$H_i = R_i \left(\begin{array}{cc} |\Lambda_{i1}| & 0 \\ 0 & |\Lambda_{i2}| \end{array} \right) R_i^{-1} \quad i \in I. \tag{27}$$

The matrices $H_i,\ i \in I$ are symmetric and positive definite. It follows from (26) and (27) , that if η is a polynom of degree less than 2 then $H_i = 0,\ i \in I$. For this case we require to have an uniform triangulation (i.e. $M_i = cI$ for all $i \in I$). This and the numerical experiments lead us to put

$$M_i = c\,[I + \alpha(\|H_i\|)H_i)] \quad i \in I, \tag{28}$$

where c is a constant and $\alpha(\|H_i\|)$ is a function of the norms of the matrix H_i. We put $\|H\| = \max_{i,j=1,2} |h_{ij}|$, where $h_{ij},\ i,j = 1,2$ are the elements of H.

Now we determine c and α. For $H_i = 0$ for all $i \in I$ (the uniform mesh) the both eigenvalues of M_i are equal to c and therefore the optimal triangulation consists of equilateral triangles with the length edge $\sqrt{3/c}$. Then

$$|T_{M_i}| = \frac{3\sqrt{3}}{4c}. \tag{29}$$

Let $|\Omega|$ denote the area of the computational domain and $nelem$ be the number of elements which we prescribe for an uniform mesh. If all triangles of the optimal triangulation are the same then we have

$$nelem \cdot |T_{M_i}| = |\Omega|. \tag{30}$$

This and (29) imply that

$$nelem \cdot \frac{3\sqrt{3}}{4c} = |\Omega| \tag{31}$$

and, hence,

$$c = \frac{3\sqrt{3}}{4}\frac{nelem}{|\Omega|}. \tag{32}$$

For the function $\alpha(\|H\|)$ we choose an empiric relation

$$\alpha(\|H_i\|) = \frac{\varepsilon_1}{\varepsilon_2 + \|H_i\|}, \quad i \in I, \tag{33}$$

where ε_1 and ε_2 are some constants. The relation (28) and (33) give

$$\lim_{\|H_i\| \to \infty} \|M_i\| = c(1 + \varepsilon_1) =: d_{\max} \quad \forall i \in I, \tag{34}$$

so the norms of $M_i,\ i \in I$ are bounded and therefore the lengths of edges of $\mathcal{T}$ are bounded from below.

Now let us determine the constants $\varepsilon_1, \varepsilon_2$. Let $H_i = 0$ for some $i \in I$. Then $M_i = cI$ and the corresponding optimal triangle has equal sides with length(in Euclidean norm)

$$l_0 = \sqrt{\frac{3}{c}}. \tag{35}$$

Let $H_i = \beta I$ for some $i \in I$ and let $\beta \gg 1$. Then $M_i \to c(1+\varepsilon_1)I$ for $\beta \to \infty$, as follows from (34) and the corresponding optimal triangle has equal sides with length(in Euclidean norm)

$$l_1 = \sqrt{\frac{3}{c(1+\varepsilon_1)}}. \tag{36}$$

It follows from (35) and (36) that the length l of any edge from the optimal triangulation $\mathcal{T}_{\text{opt}}$ satisfies (provided M_i is defined by (28) and (33))

$$l_1 = \sqrt{\frac{3}{c(1+\varepsilon_1)}} \leq l \leq \sqrt{\frac{3}{c}} = l_0. \tag{37}$$

It can be shown that the values l_0 and l_1 are the maximal and minimal lengths of an edge of an optimal triangulation, respectively. The value l_0 is given by (35) and (30) (where we prescribe $nelem$). It follows from (37) that

$$\frac{l_0}{l_1} = \sqrt{c(1+\varepsilon_1)} \Longrightarrow \varepsilon_1 = \left(\frac{l_0}{l_1}\right)^2 - 1. \tag{38}$$

Relation (38) shows what role plays the constant ε_1. The quotient $\frac{l_0}{l_1}$ performs the ratio between the longest and the shortest edge admissible in the optimal triangulation. If we

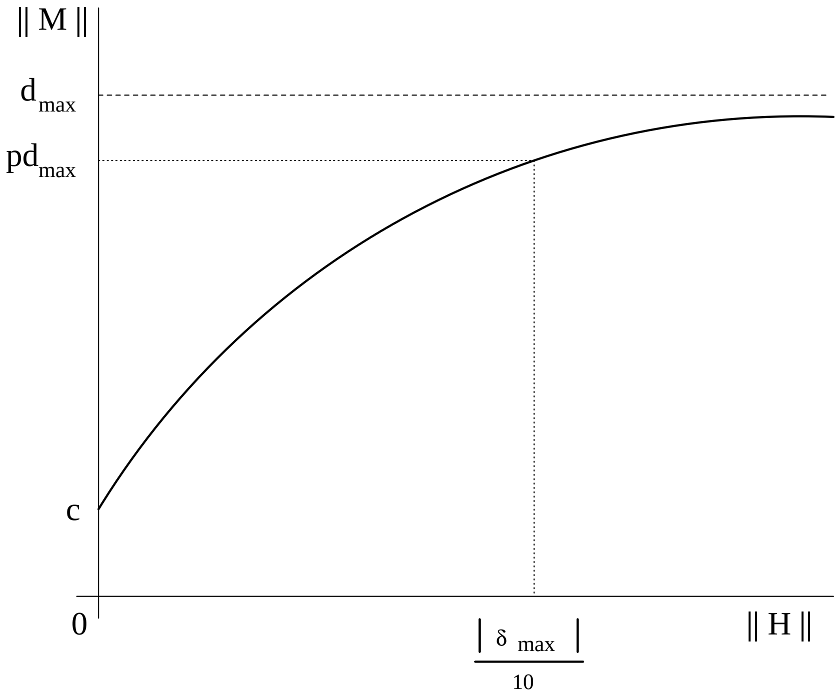

Figure 9: Dependence $\|M\|$ on $\|H\|$ given by (28) and (33).

prescribe the ratio $\frac{l_0}{l_1}$ (we set in our code $\frac{l_0}{l_1} = 100$), then (38) gives the value of ε_1. For ε_2 we use the following empiric relation

$$\varepsilon_2 = \frac{1}{10}|\delta_{\max}| \frac{(\varepsilon_1 + 1)(1 - p)}{p(\varepsilon_1 + 1) - 1}, \tag{39}$$

where $|\delta_{\max}| = \frac{1}{l_1^2}$ which estimates the maximal second order derivative for the optimal triangulation and $p \in (0, 1)$. We put $p = 0.8 - 0.95$. This condition prescribes that for $\|H\| = |\delta_{\max}|/10$ we have $\|M\| = pc(1 + \varepsilon_1) = pd_{\max}$. The significance of (39) can be seen on Fig. 9.

6.1 Computation of the second order derivatives

We need to know the values of the second order derivative of the function η at each node of $\mathcal{T}$ for the relations (26). We approximate η by a piecewise linear function η_h. Let X_h be a space of continuous and piecewise linear functions on each triangle from $\mathcal{T}$ and $V_h = \{\psi,\ \psi \in X_h,\ \psi|_{\partial\Omega} = 0\}$. Let $\eta_h \in X_h$. It is necessary to evaluate the second order derivative of η_h, i.e. $\partial^2\eta_h/\partial x^2$, $\partial^2\eta_h/\partial x\partial y$ and $\partial^2\eta_h/\partial y^2$ which do not exist in the classical sense. We approximate $\partial^2\eta_h/\partial x^2$ by a function $D^2\eta_h \in X_h$ such that

$$\left(\frac{\partial^2\eta_h}{\partial x^2}, \varphi\right) \approx \left(D^2\eta_h, \varphi\right) = -\left(\frac{\partial\eta_h}{\partial x}\frac{\partial\varphi}{\partial x}\right) \quad \forall\varphi \in V_h, \tag{40}$$

where $(\cdot,\cdot)$ means the scalar product in $L^2(\Omega_h)$. For boundary nodes we use an extrapolation from the interior part of the computational domain. The R.H.S. of (40) has already sense because $\eta_h, \varphi \in V_h$ and therefore the first derivatives exist and are piecewise constant. We choose the special subset of test functions $\{\varphi_i, \varphi_i \in V_h, \varphi_i(P_j) = \delta_{ij}, i, j \in I\}$, where $P_j,\ j \in I$ are nodes from $\mathcal{T}$ and δ_{ij} is the Kronecker delta.

The R.H.S. of (40) gives

$$\left(\frac{\partial \eta_h}{\partial x}, \frac{\partial \varphi_i}{\partial x}\right) = \sum_{T \in \mathcal{T}} |T| \frac{\partial \eta_h}{\partial x}\bigg|_T \frac{\partial \varphi_i}{\partial x}\bigg|_T = \sum_{T \in d(i)} |T| \frac{\partial \eta_h}{\partial x}\bigg|_T \frac{\partial \varphi_i}{\partial x}\bigg|_T \quad i \in I, \tag{41}$$

where $d(i),\ i \in I$ is a set of triangles which has P_i as a vertex.

The L.H.S. of (40) gives

$$\left(D^2\eta_h, \varphi_i\right) = \sum_{T \in \mathcal{T}} \int_T D^2 \eta_h \varphi_i \ dx. \tag{42}$$

We use the "mass lumping" numerical quadrature

$$\int_T F \ dx \approx \frac{1}{3}|T| \sum_{n=1}^{3} F(P_n^T), \tag{43}$$

where $F \in C(T)$ and $P_n^T,\ n = 1, 2, 3$ are the vertices of T. From (42) and (43) we have

$$\begin{aligned} \left(D^2\eta_h, \varphi_i\right) &= \sum_{T \in \mathcal{T}} \frac{1}{3}|T| \sum_{m=1}^{3} D^2\eta_h(P_m^T)\varphi_i(P_m^T) = \qquad (44)\\ &= \sum_{T \in d(i)} \frac{1}{3}|T| \sum_{m=1}^{3} D^2\eta_h(P_m^T)\varphi_i(P_m^T) = \frac{1}{3}D^2\eta_h(P_i) \sum_{T \in d(i)} |T|. \end{aligned}$$

It is easy to show that $\frac{1}{3}\sum_{T \in d(i)} |T| = |D_i|$, where $|D(i)|$ is the area of the so-called dual finite volume (Fig. 10) associated with the vertex P_i (see, e.g. [5],[6]).

The relations (40), (41) and (44) yield

$$\frac{\partial^2 \eta_h}{\partial x^2}(P_i) \approx D^2\eta_h(P_i) = -\frac{1}{|D_i|} \sum_{T \in d(i)} |T| \frac{\partial \eta_h}{\partial x}\bigg|_T \frac{\partial \varphi_i}{\partial x}\bigg|_T \quad i \in I. \tag{45}$$

Similarly we obtain

$$\frac{\partial^2 \eta_h}{\partial x \partial y}(P_i) \approx -\frac{1}{|D_i|} \sum_{T \in d(i)} |T| \frac{\partial \eta_h}{\partial x}\bigg|_T \frac{\partial \varphi_i}{\partial y}\bigg|_T \quad i \in I, \tag{46}$$

$$\frac{\partial^2 \eta_h}{\partial y \partial x}(P_i) \approx -\frac{1}{|D_i|} \sum_{T \in d(i)} |T| \frac{\partial \eta_h}{\partial y}\bigg|_T \frac{\partial \varphi_i}{\partial x}\bigg|_T \quad i \in I, \tag{47}$$

and

$$\frac{\partial^2 \eta_h}{\partial y^2}(P_i) \approx -\frac{1}{|D_i|} \sum_{T \in d(i)} |T| \frac{\partial \eta_h}{\partial y}\bigg|_T \frac{\partial \varphi_i}{\partial y}\bigg|_T \quad i \in I. \tag{48}$$

We also need to prove that (46) and (47) give the same value, i.e. we must prove

$$\begin{aligned} &\left(\left(\frac{\partial \eta_h}{\partial x}, \frac{\partial \varphi_i}{\partial y}\right) =\right) \sum_{T \in d(i)} |T| \frac{\partial \eta_h}{\partial x}\bigg|_T \frac{\partial \varphi_i}{\partial y}\bigg|_T = \qquad (49)\\ &= \sum_{T \in d(i)} |T| \frac{\partial \eta_h}{\partial y}\bigg|_T \frac{\partial \varphi_i}{\partial x}\bigg|_T \left(= \left(\frac{\partial \eta_h}{\partial y}, \frac{\partial \varphi_i}{\partial x}\right)\right) \quad \forall i \in I, \end{aligned}$$

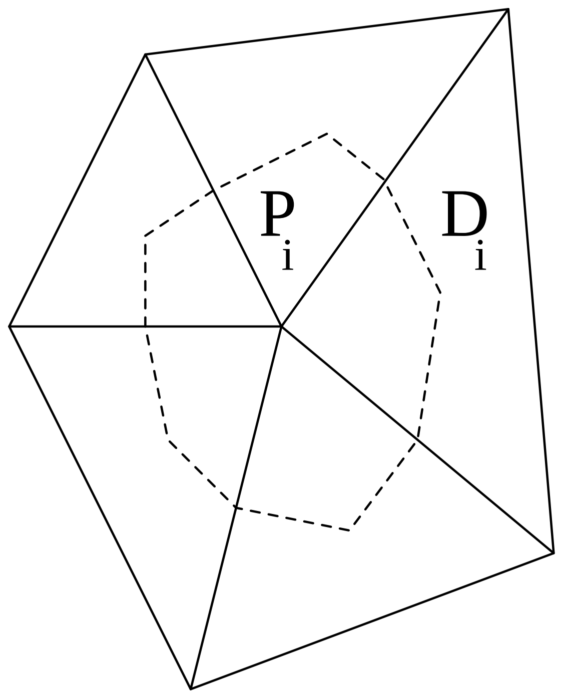

Figure 10: The control volume D_i corresponding to node P_i.

As $\eta_h \in X_h$ then we can write

$$\eta_h(x) = \sum_{j \in I} \eta_h(P_j)\varphi_j(x). \tag{50}$$

Therefore it is enough to prove that

$$\left(\frac{\partial \varphi_i}{\partial x}, \frac{\partial \varphi_j}{\partial y}\right) = \left(\frac{\partial \varphi_i}{\partial y}, \frac{\partial \varphi_j}{\partial x}\right) \qquad i, j \in I. \tag{51}$$

For the case $i = j$ the relation (51) is evident. If P_i and P_j are not vertices of a common triangle T then the scalar products in (51) are equal to 0 because the supports of the functions φ_i and φ_j are disjoint. Now it is enough to prove (49) for the case when P_i and P_j form an edge of some $T \in \mathcal{T}$ (see Fig. 11).

Let $P_i = (x_i, y_i)$, $P_j = (x_j, y_j)$, $P_k = (x_k, y_k)$, $P_l = (x_l, y_l)$ are nodes and T_1, T_2 are neighbouring triangles with the common edge P_iP_j, see Fig. 11. Then the relation (51) can be rewritten as

$$\int_{T_1} \frac{\partial \varphi_i}{\partial x}\frac{\partial \varphi_j}{\partial y}\, dx + \int_{T_2} \frac{\partial \varphi_i}{\partial x}\frac{\partial \varphi_j}{\partial y}\, dx = \int_{T_1} \frac{\partial \varphi_i}{\partial y}\frac{\partial \varphi_j}{\partial x}\, dx + \int_{T_2} \frac{\partial \varphi_i}{\partial y}\frac{\partial \varphi_j}{\partial x}\, dx. \tag{52}$$

Using the standard results (Cf., e.q., [7], Section 4.4) we obtain

$$\begin{aligned}
\left.\frac{\partial \varphi_i}{\partial x}\right|_{T_1} &= \frac{y_k - y_j}{2|T_1|}, & \left.\frac{\partial \varphi_i}{\partial x}\right|_{T_2} &= \frac{y_j - y_l}{2|T_2|}, & \left.\frac{\partial \varphi_i}{\partial y}\right|_{T_1} &= \frac{x_j - x_k}{2|T_1|}, & \left.\frac{\partial \varphi_i}{\partial y}\right|_{T_2} &= \frac{x_l - x_j}{2|T_2|} \\
\left.\frac{\partial \varphi_j}{\partial x}\right|_{T_1} &= \frac{y_i - y_k}{2|T_1|}, & \left.\frac{\partial \varphi_j}{\partial x}\right|_{T_2} &= \frac{y_l - y_i}{2|T_2|}, & \left.\frac{\partial \varphi_j}{\partial y}\right|_{T_1} &= \frac{x_k - x_i}{2|T_1|}, & \left.\frac{\partial \varphi_j}{\partial y}\right|_{T_2} &= \frac{x_i - x_l}{2|T_2|},
\end{aligned} \tag{53}$$

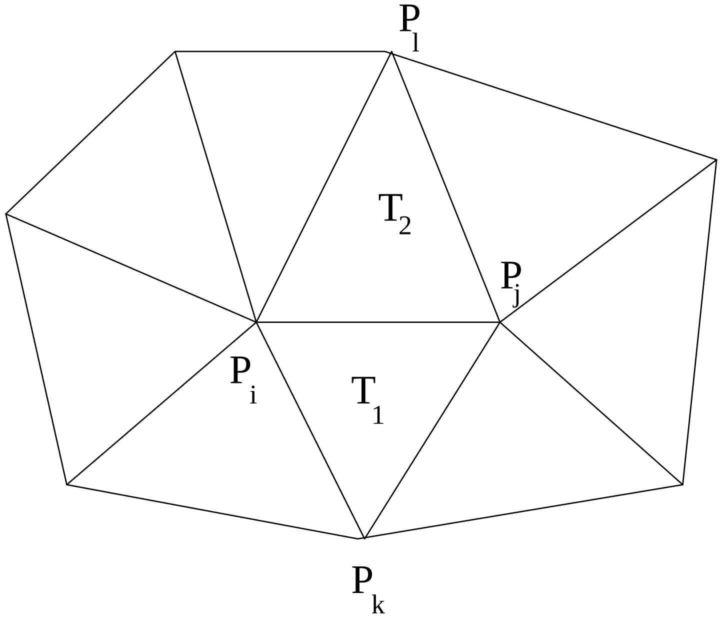

Figure 11: The notation for the prove of (49). Triangle T_1 formed by $P_iP_jP_l$ and T_2 by $P_jP_iP_k$.

where

$$2|T_1| = \begin{vmatrix} x_i & y_i & 1 \\ x_k & y_k & 1 \\ x_j & y_j & 1 \end{vmatrix}, \qquad 2|T_2| = \begin{vmatrix} x_i & y_i & 1 \\ x_j & y_j & 1 \\ x_l & y_l & 1 \end{vmatrix}. \tag{54}$$

Now putting (53) and (54) into (52), we arrive after a lengthy calculation at (49), which we wanted to prove.

7 Multilevel computation

The technique described above is applied in the following way: We start from an initial very coarse triangulation of a suitable polygonal approximation of the computational domain (for example, see Fig. 12). Now we can generate a triangulation $\mathcal{T}_0$, using AMA described in Section 5, as a uniform triangulation ($M_i = cI,\ i \in I$) with c given by (30), where $nelem$ represents the number of elements which we prescribe for the triangulation $\mathcal{T}_0$ (for example 500, see Fig. 12). In practice, during the generation of a triangulation we do not achieve the prescribed number of elements. The number of triangles is 16 for the initial triangulation and 536 for $\mathcal{T}_0$ (Fig. 12).

We compute the solution W_0 on the triangulation $\mathcal{T}_0$, using a numerical method suitable for the problem of consideration (FVM, FEM, ...). With the aid of (26) – (28), we compute the matrices M_i from W_0 at each node of $\mathcal{T}_0$ and, using the iterative process from Section 5, we construct the triangulation $\mathcal{T}_1$. The results from $\mathcal{T}_0$ are transferred onto $\mathcal{T}_1$ and the computation can continue. Then we obtain W_1. (In general we pass from $\mathcal{T}_k$ to $\mathcal{T}_{k+1}$ in the same way.) We obtain, consecutively, $\mathcal{T}_0, \mathcal{T}_1, \mathcal{T}_2, \ldots$ and $W_0, W_1, W_2, \ldots$. There is a natural question when to stop this process. Numerical experiments show that for given $nelem$, ε_1, ε_2,

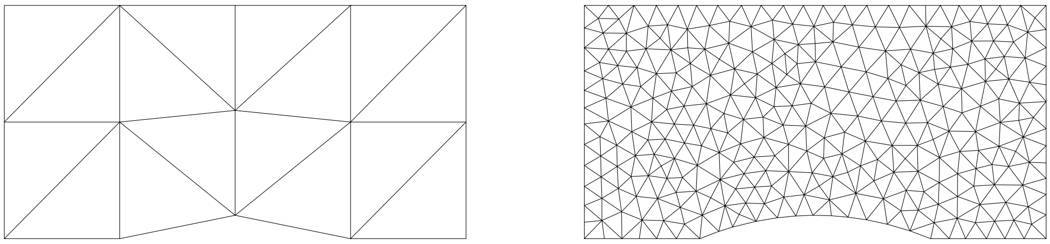

Figure 12: Initial mesh for AMA (left) and the mesh $\mathcal{T}_0$ constructed by AMA (right).

"the computation converges", i.e., there exists a number k for which the triangulations $\mathcal{T}_k$ and $\mathcal{T}_{k+1}$ are (approximately) the same. The number k is approximately between 5 and 8 for our problems. From numerical experiments follows that the generation of triangulations using AMA needs at most 5% of the total CPU–time of the complete computational process.

8 Numerical examples

Here we are concerned with inviscid compressible flow through the GAMM channel with the inlet Mach number $M_{\text{in}} = 0.67$. We present the mesh obtained after 4 refinements (Fig. 13), the corresponding isolines of the Mach number (Fig. 14), and the color map of the Mach number (Fig. 15). We use $nelem = 500$, $\varepsilon_1 = 10000$, and $p = 0.98$. Fig. 16, Fig. 17, and Fig. 18 show the results obtained by the standard red–green refinement technique based on a shock indicator [8]. Fig. 19 presents the distributions of the Mach number along the solid walls.

The following table compares both of the adaptative methods:

type of the method	AMA	red – green
CPU – time	1570 s	2274 s
total number of levels of mesh adaptations	4	4
number of elements for the last level of adaptation	4601	4731

We see that whereas the numbers of elements for the last level of refinement are approximately the same, the CPU–time is essentially lower for the AMA technique. Moreover, Figs. 14, 15, 17, 18 and 19 show that the sharpness of shock waves is greater for AMA, i.e., the results obtained by AMA have a better quality.

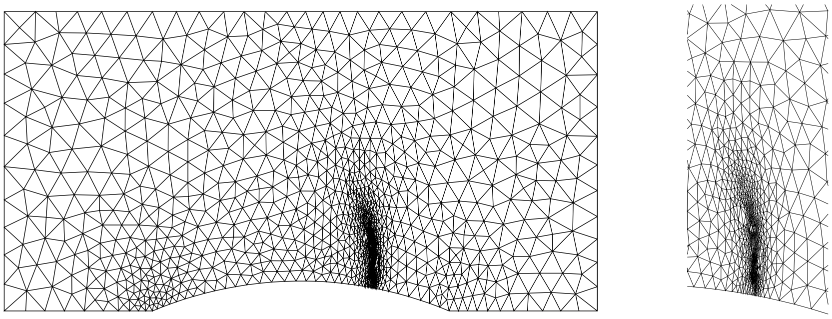

Figure 13: Mesh after fourth refinement and its detail obtained by AMA.

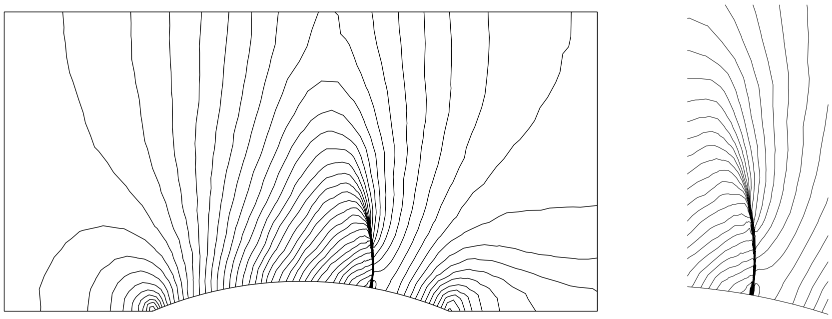

Figure 14: Isolines of Mach number after fourth refinement and its detail obtained by AMA.

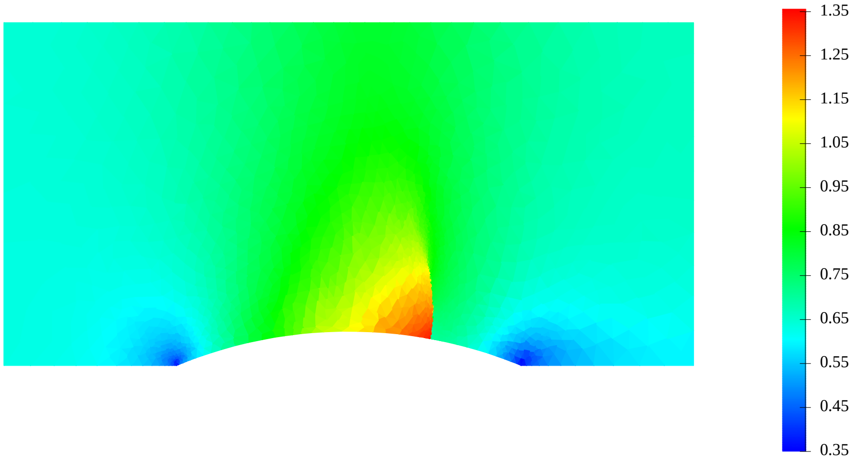

Figure 15: The map of piecewise linear distribution of Mach number after fourth refinement obtained by AMA.

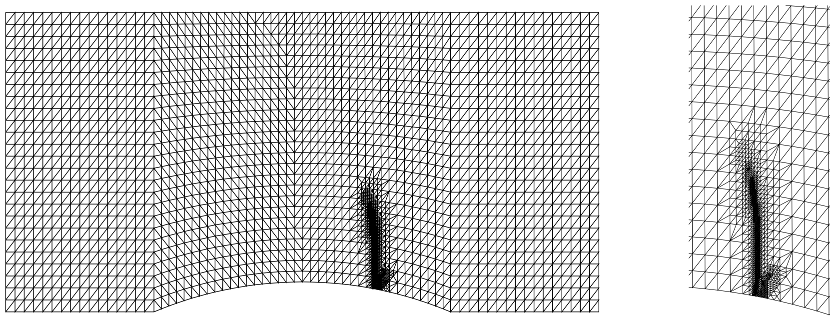

Figure 16: Mesh after fourth refinement and its detail obtained by red–green refinement.

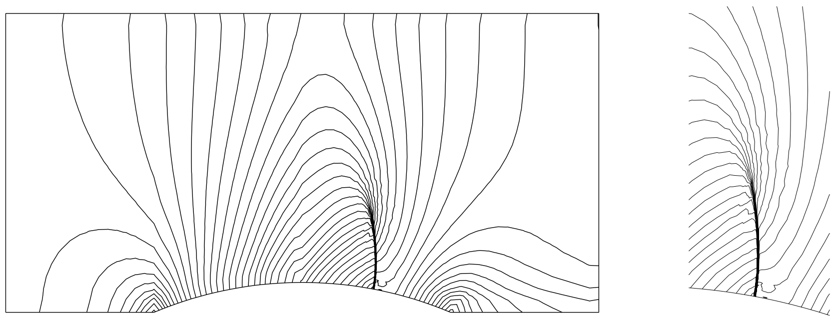

Figure 17: Isolines of Mach number after fourth refinement and its detail obtained by red–green refinement.

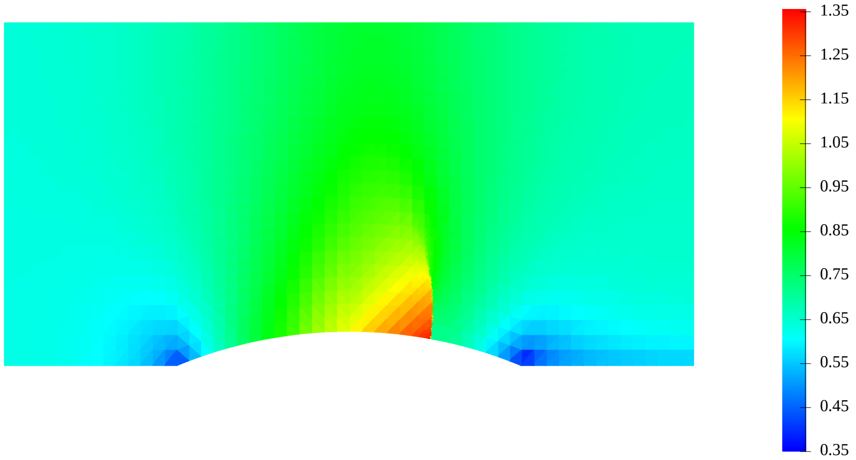

Figure 18: The map of piecewise linear distribution of Mach number after fourth refinement obtained by red–green refinement.

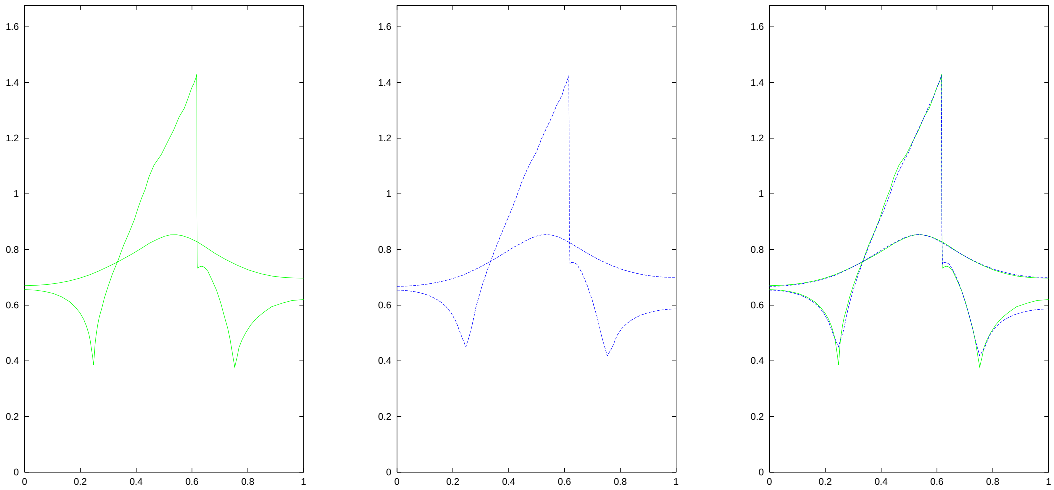

a b c

Figure 19: Distribution of Mach number a) obtained by AMA, b) obtained by red – green refinement, c) both of them.

As the second example we present the simulation of the flow around NACA 0012 profile with the inlet Mach number $M_{\text{in}} = 0.8$ and angle of attack $\alpha = 0$. An adaptation was performed of the mesh by AMA with $c = 500$, $\varepsilon_1 = 10000$ and $p = 0.95$. The Figs. 20, 21, 22, 23, and 24 show the triangulations and the maps of the Mach number of the successive mesh adaptation for the zeroth, first, second, fourth, and sixth level of refinement, respectively. Wee see that from very poor results obtained for the initial triangulation we obtain good results with very sharp shock waves. The results for the fourth and sixth level of refinement (Fig. 23 and Fig. 24) are almost identical, which corresponds to the assertion that the AMA algorithm "converges" (see Section 7). A slight asymmetry of the maps of the Mach number is given by the asymmetry of triangulation, which follows from the fact that AMA is an iterative method. To avoid this asymmetry it is necessary to construct the AMA code in such a way that the symmetry prescribed should be preserved.

Acknowledgements

This work was supported by Grant No. 201/96/0313 of the Grant Agency of Czech Republic. The author gratefully acknowledges this support.

References

[1] M. J. Castro Díaz, H. Borouchaki, P. L. George, F. Hecht, and B. Mohammadi. Anisotropic Adaptive Mesch Generation in Two Dimensions for CFD. In *Proceeding of ECCOMAS96 – Computational Fluid Dynamics, Paris*, pages 181–186, 1996.

[2] H. Borouchaki, P. L. George, F. Hecht, P. Laugh, and E. Saltel. Mailleur bidimensionnal de Delaunay gouverné par une carte de métriques. Partie I: Algorithmes. Technical Report 2741, INRIA, 1995.

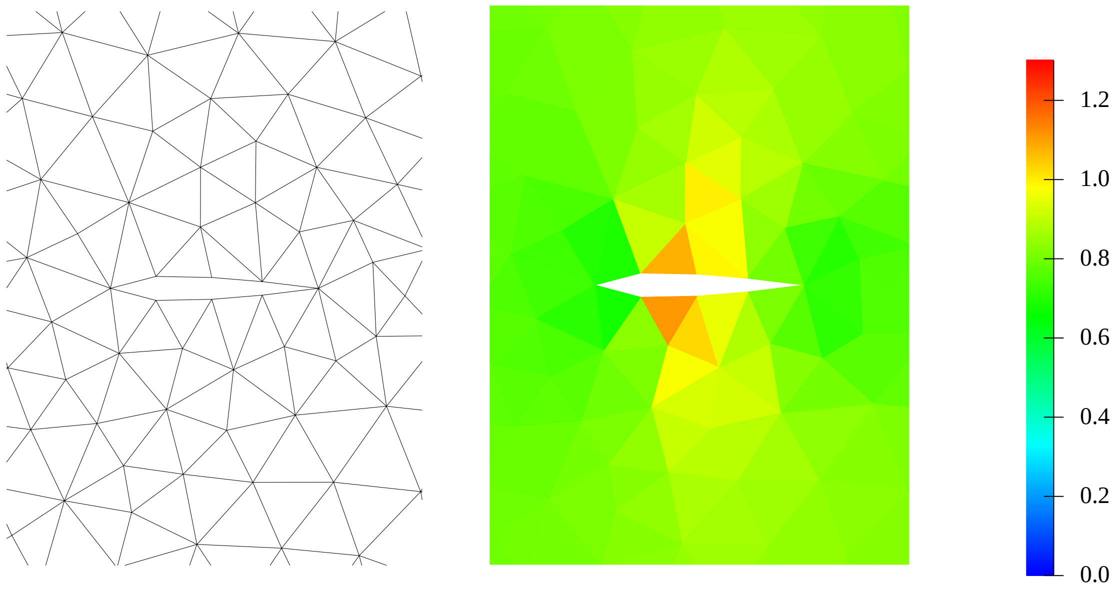

Figure 20: Mesh and map of Mach number around NACA0012 after the zeroth adaptation.

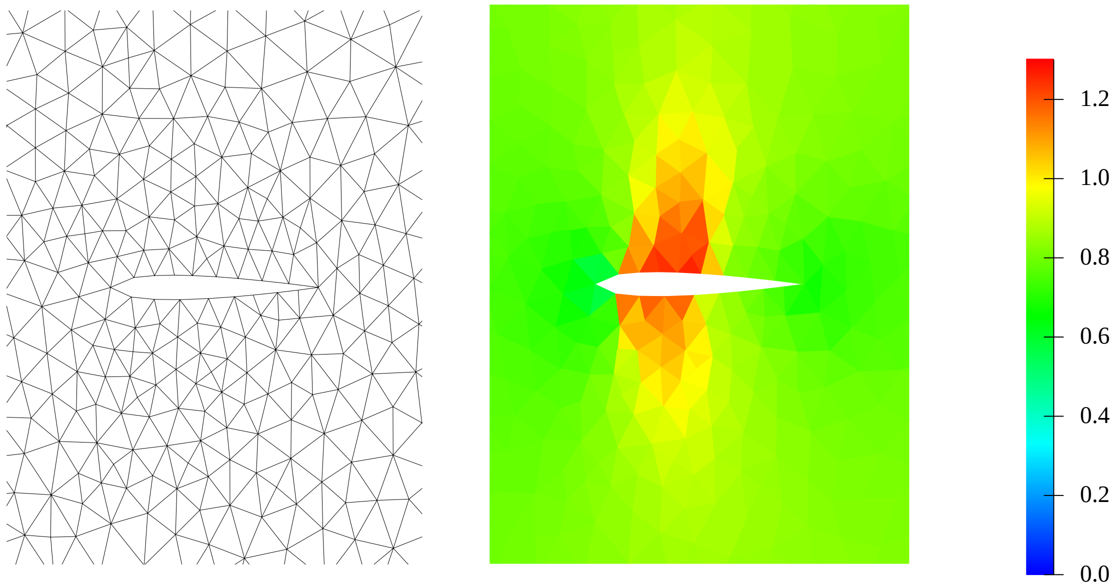

Figure 21: Mesh and map of Mach number around NACA0012 the after first adaptation.

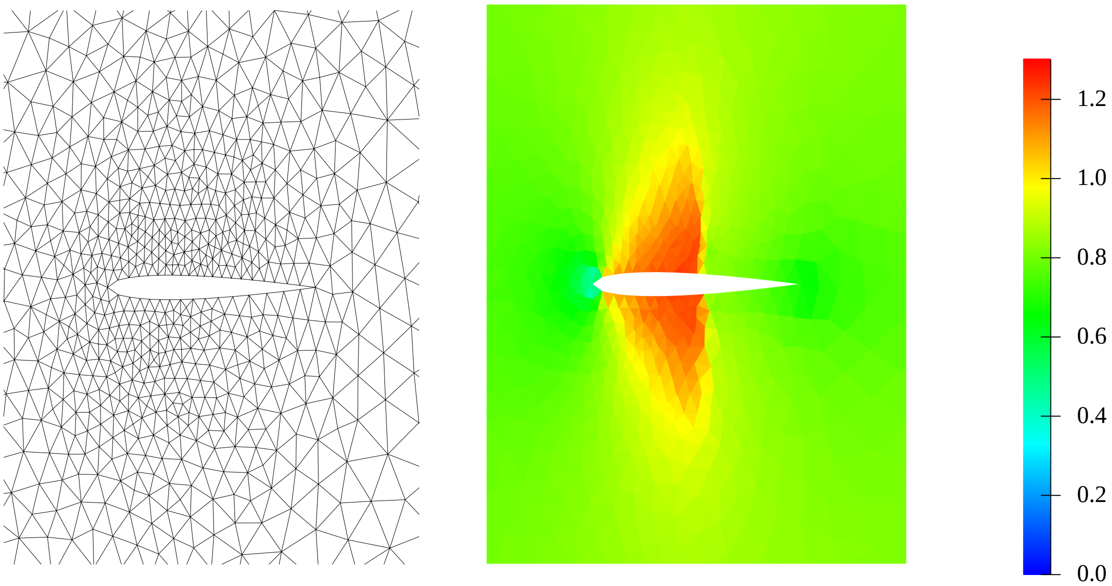

Figure 22: Mesh and map of Mach number around NACA0012 after the second adaptation.

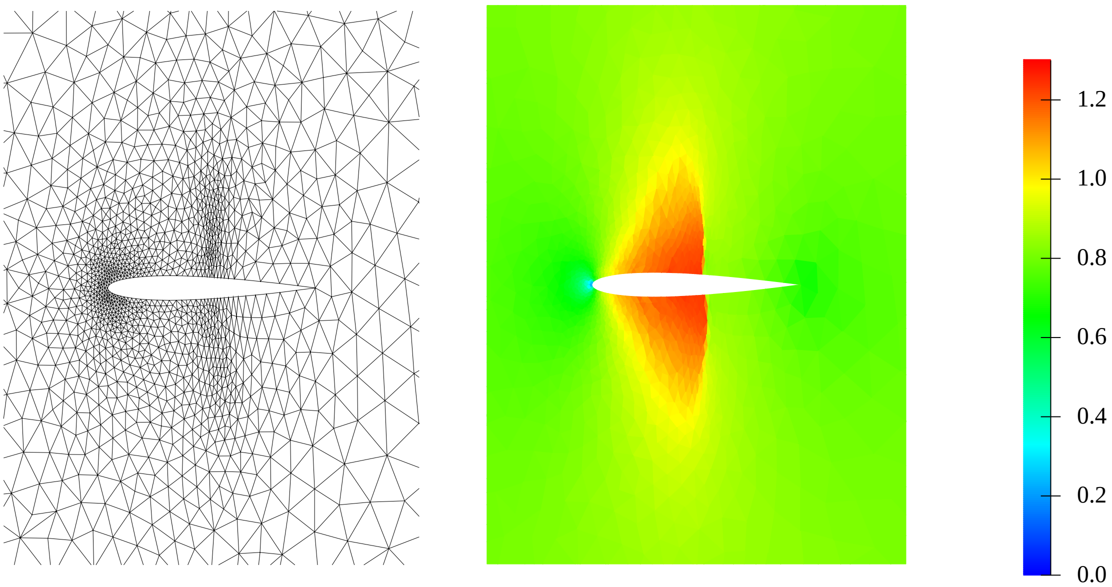

Figure 23: Mesh and map of Mach number around NACA0012 after the fourth adaptation.

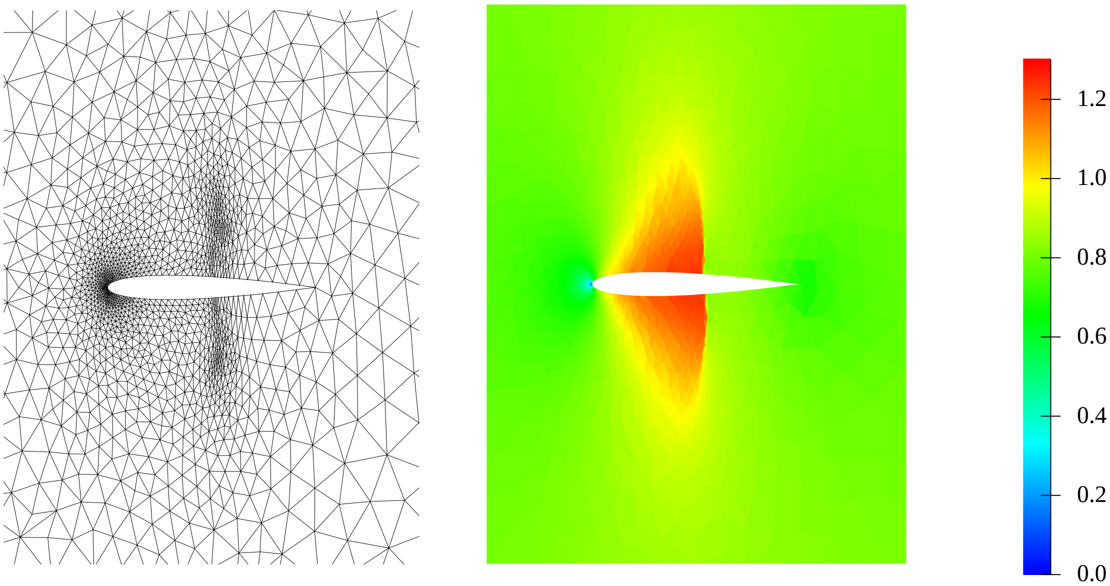

Figure 24: Mesh and map of Mach number around NACA0012 after the sixth adaptation.

[3] P. G. Ciarlet. *The Finite Elements Method for Elliptic Problems.* North-Holland, Amsterodam, 1979.

[4] E. F. D'Azevedo and R. B. Simpson. On optimal triangular meshes for minimizing the gradient error. *Numer. Math.*, 59:321–348, 1991.

[5] M. Feistauer and J. Felcman. Convection-Diffusion Problems and Compressible Navier–Stokes Equations. In J. R. Whitemen, editor, *The Mathematics of Finite Elements and Applications*, pages 175–194. John Wiley & Sons, 1996.

[6] M. Feistauer, J. Felcman, and M. Lukáčová. Combined finite elements–finite volume solution of compressible flow. *Journal of Comput. and Applied Math.*, 63:179–199, 1995.

[7] M. Feistauer, J. Felcman, M. Rokyta, and Z. Vlášek. Finite element solution of flow problems with trailing conditions. *J. Comput. Appl. Math*, 44:131–145, 1992.

[8] J. Felcman and V. Dolejší. Adaptive Methods in Internal and External Flow Computations. In M. P. Bendsøe M. Brøns and M. P. Sørensen, editors, *Progress in Industrial Mathematics at ECMI 96*, pages 424–431. B. G. Teubner, Stuttgart, 1997. ISBN 3-519-02607-4.

[9] M. Fortin, M.-G. Vallet, J. Dompierre, Y. Bourgault, and W. G. Habashi. Anisotropic Mesch Adaptation: Theory, Validation and Applications. In *Proceeding of ECCOMAS96 – Computational Fluid Dynamics, Paris*, pages 174–180, 1996.